

# Work-minimizing kinematics of a flat plate moving parallel to its surface in a fluid

S. Mandre\*

*Mathematics Institute, University of Warwick, Coventry UK CV4 7AL*

(Dated: October 19, 2024)

## Abstract

The minimum work needed to translate a thin flat plate immersed in a fluid a given distance  $D$  parallel to its surface in a fixed duration  $T$  is calculated. The Reynolds number for the flow is assumed to be large so that the drag on the plate arises from skin friction. The plate starts from rest with speed  $\propto t^{1/4}$  and comes to rest with speed  $\propto (T - t)^{1/4}$ . For distances much longer than the plate, the work-minimizing kinematics consists of an optimum startup, cruising at a constant speed, and an optimum stopping.

arXiv:2006.02152v1 [physics.flu-dyn] 3 Jun 2020

---

\* Corresponding author: shreyas.mandre@warwick.ac.uk

Applications of kinematic optimization in the presence of fluids include animal propulsion ranging from hovering flight[1] to swimming in flagellated microorganisms[2], jellyfish[3], and fish[4]. Powerful solution techniques are available in the limit where viscous forces dominate over inertial ones[2, 5–11], which renders the governing equations linear and kinematically reversible. These techniques do not apply to the situation we consider in this article when inertia dominates and the nonlinearities cannot be ignored. In this case, due to the difficulties posed by the nonlinearities and the appearances of multiple scales, methods based on calculus of variations are avoided. Instead, the kinematics are usually parameterized to a finite-dimensional space, and the parameters optimized[3, 4, 12–15]. One such difficulty – the gradient evaluation that requires the adjoint equations to be integrated backwards in time – is logistical, and recent computational hardware and software has begun to overcome it for computational fluid mechanics[16–19]. But in the absence of a theory of fluid mechanical kinematic optimization, a fundamental challenge that remains is the possible presence of local optima in which an iterative solution method could be trapped.

In this article, we determine the profile of transient speed  $V(\tilde{t})$  with time  $\tilde{t}$  of a flat plate of length  $L$  moving parallel to its surface a distance  $D$  in time  $T$  (see Figure 1) that minimizes the mechanical work  $\tilde{W}$ . (The work-minimizing kinematics also solves two related problems: maximizing  $D$  given  $T$  and  $\tilde{W}$ , and minimizing  $T$  given  $D$  and  $\tilde{W}$  – the fluid dynamical brachistochrone.) The surrounding fluid of density  $\rho$  and viscosity  $\mu$  is of infinite extent and initially static. The plate is infinitesimal in its thickness and infinitely long in the third dimension so that the resulting flow is two-dimensional in character. In the limit  $\text{Re} = \rho LD / (T\mu) \gg 1$ , a thin viscous boundary layer governs the drag. The dynamics in the boundary layer are transient and nonlinear, so changes made to the kinematics at one instance have an influence on the drag for all subsequent times.

The second dimensionless parameter,  $\epsilon = D/L$ , represents the target distance to be travelled relative to the plate length. For short distances travelled, i.e.  $\epsilon \ll 1$ , the nonlinearities in the fluid dynamics are eliminated, the optimum is unique, and even an analytical solution is possible[20]. But the problem for finite or large  $\epsilon$ , where the fluid dynamical nonlinearities pose the aforementioned difficulties, has not been solved to date.

We consider the regime for  $\text{Re} \gg 1$  and arbitrary  $\epsilon$  in this article. Using calculus of variations, we determine the minimum-work kinematics for laminar flow in this regime. For small  $\epsilon$ , the analytical solution in Ref. [20] is recovered. For large  $\epsilon$ , the work-minimizing

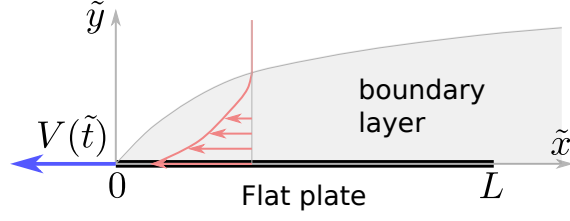


FIG. 1. Schematic a flat plate moving through a fluid.

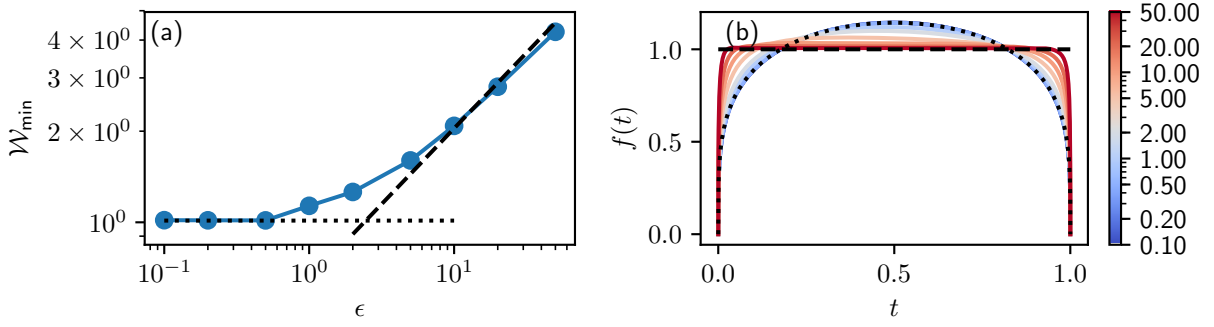


FIG. 2. Minimum work for translating a flat plate and the corresponding optimal  $f(t)$ . (a)  $\mathcal{W}_{\min}$  as a function of  $\epsilon$ . The dotted line shows  $\mathcal{W}_{0,\min} \approx 1.014$  from (12b) and the dashed lines shows  $0.664\epsilon^{1/2}$ . (b)  $f(t)$  for different  $\epsilon$  coded according to the color in the adjoining colorbar. Dotted curve shows  $f_0(t)$  from (12a) and the dashed curve shows unity.

kinematics comprises an optimal start-up dynamics, followed by cruising at a constant speed  $V(\tilde{t}) \approx D/T$ , followed by an optimal stopping dynamics. The optimal plate speed starts from rest as  $V(\tilde{t}) \propto \tilde{t}^{1/4}$  for  $\tilde{t} \ll \epsilon T$ , and comes to a complete stop at the end as  $V(\tilde{t}) \propto (T - \tilde{t})^{1/4}$  for  $T - \tilde{t} \ll \epsilon T$ . The minimum work needed asymptotically approaches  $\mathcal{W}_{\min} \approx 0.664\sqrt{\mu\rho D^5 L/T^3}$  as  $\epsilon \rightarrow \infty$ . Remarkably, despite the nonlinear nature of the fluid dynamics, the optimum is unique and, therefore, global. We provide a physical rationale for the optimum kinematics as well as the uniqueness result.

The fluid outside a thin boundary layer, to leading order in  $\text{Re}$ , remains stationary as the plate moves. We use a coordinate system attached to the leading edge of the plate, as shown in Figure 1, and a reference frame attached to farfield stationary fluid. Exploiting the reflection symmetry, we only consider the flow field for  $y \geq 0$  and the drag on one face of the plate. The coordinate  $\tilde{x}, \tilde{y}$  and the flow velocity  $(\tilde{u}(\tilde{x}, \tilde{y}, \tilde{t}), \tilde{v}(\tilde{x}, \tilde{y}, \tilde{t}))$  in the boundary

layer are non-dimensionalized as

$$\tilde{t} = Tt, \quad \tilde{x} = Lx, \quad \tilde{y} = \delta y, \quad \tilde{u} = \frac{D}{T}u, \quad \tilde{v} = \frac{D\delta}{TL}v, \quad (1)$$

where  $\delta = \sqrt{\nu T}$  to yield the dimensionless form of the governing boundary layer equations as

$$\mathcal{M} = u_t + \epsilon(u + f)u_x + \epsilon v u_y - u_{yy} = 0, \quad (2a)$$

$$\mathcal{C} = u_x + v_y = 0, \quad (2b)$$

in the semi-infinite half-space  $y \geq 0$  and

$$u_{x \in P, y=0} + f(t) = u_y|_{x \notin P, y=0} = 0, \quad (3a)$$

$$u|_{y=\infty} = u|_{x=-\infty} = u|_{t=0} = 0, \quad (3b)$$

where  $P = [0, 1]$ ,  $f = (T/D)V(\tilde{t})$  is the dimensionless plate speed, which satisfies the condition for total distance traveled as

$$\mathcal{D} = \int_0^1 f(t) dt - 1 = 0. \quad (4)$$

The work done is  $\tilde{\mathcal{W}} = D^2 L \sqrt{\mu \rho / T^3} \mathcal{W}[f]$ , where

$$\mathcal{W}[f] = \int_0^1 \int_0^1 f(t) u_y(x, y=0, t) dx dt. \quad (5)$$

Within the framework of the boundary layer approximation, the work done must appear as an increase in the kinetic energy of the fluid or be viscously dissipate, i.e.,

$$\mathcal{W}[f] = \int_{-\infty}^{\infty} \int_0^{\infty} \left[ \frac{(u + f)^2|_{t=1}}{2} + \int_0^1 u_y^2 dt \right] dy dx. \quad (6)$$

The objective of the optimization is to minimize  $\mathcal{W}[f]$  subject to  $\mathcal{M} = \mathcal{C} = 0$  in the fluid. The corresponding Lagrangian is

$$\mathcal{L} = \mathcal{W}[f] - \int_0^1 \int_{-\infty}^{\infty} \int_0^{\infty} (\alpha \mathcal{M} + \epsilon \beta \mathcal{C}) dy dx dt - \lambda \mathcal{D} \quad (7)$$

where  $\alpha(x, y, t)$ ,  $\beta(x, y, t)$ , and  $\lambda$  are Lagrange multipliers. The multipliers  $\alpha$  and  $\beta$  satisfy the condition that first variations of  $\mathcal{L}$  due to  $u$  and  $v$  vanish, i.e.,

$$\alpha_t + \epsilon(u + f)\alpha_x + \epsilon(v\alpha)_y + \epsilon\beta_x + \alpha_{yy} = 0, \quad (8a)$$

$$\beta_y = \alpha u_y, \quad (8b)$$

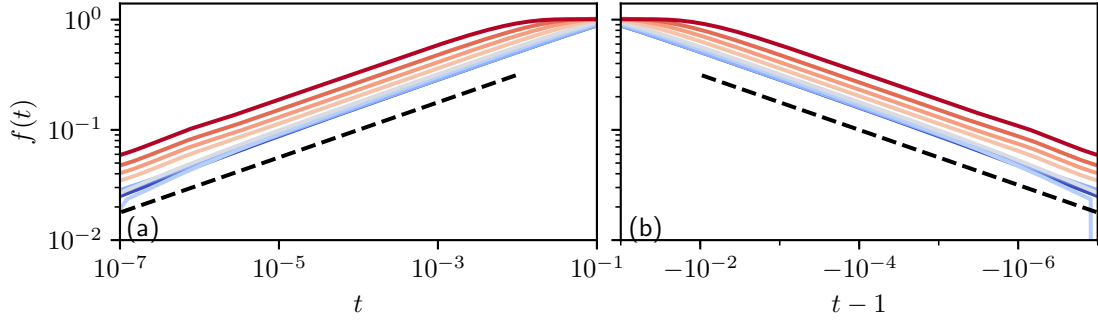


FIG. 3. Optimal starting and stopping kinematics plotted on a logarithmic scale. (a) Starting kinematics. Color code identical to that in Figure 2. Dashed line shows  $t^{1/4}$ . (b) Stopping kinematics. Dashed line shows  $(T - t)^{1/4}$ .

in  $y > 0$  subject to the boundary conditions

$$\alpha|_{x \in P, y=0} - f(t) = \alpha_y|_{x \notin P, y=0} = 0, \quad (9a)$$

$$\alpha|_{y=\infty} = \alpha|_{x=\infty} = \alpha|_{t=1} = 0, \quad (9b)$$

The first variation with respect to  $f$  given by

$$\frac{\delta \mathcal{L}}{\delta f} = \int_0^1 [u_y - \alpha_y]_{y=0} dx - \epsilon \int_{-\infty}^{\infty} \int_0^{\infty} \alpha u_x dy dx - \lambda \quad (10)$$

must also vanish.

Remarkably, despite the nonlinearities in the governing fluid dynamics, the profile  $f(t)$  that satisfies the first-order optimality condition is unique and hence the global minimum. To see this, consider the variation for a *finite* perturbation  $\delta f$  to  $f^*$ , and the corresponding perturbation  $\delta u$  to  $u^*$ , where  $f^*$  and  $u^*$  satisfy the first order optimality conditions. The positive definiteness of  $\delta \mathcal{W} = \mathcal{W}[f^* + \delta f] - \mathcal{W}[f^*]$  is most readily seen by substituting in (6), which yields

$$\delta \mathcal{W} = \int_{-\infty}^{\infty} \int_0^{\infty} \left[ \frac{(\delta u + \delta f)^2|_{t=1}}{2} + \int_0^1 \delta u_y^2 dt \right] dy dx, \quad (11)$$

implying that any perturbations to  $f^*$  necessarily increases the resulting  $\mathcal{W}$ . Solution of the first-order optimality conditions is therefore unique and yields the global optimum.

Since no analytical solution to (2), (3), (8), (9) and (10) is known for a general  $f(t)$ , the stationary profiles are determined numerically as follows. Equations (2) are discretized on a fixed non-uniform grid in  $t$ ,  $y$  and  $x$ , such that grid points are clustered closer to  $t = 0$

and 1,  $y = 0$  and  $x = 0$  and 1. (A number of different clustering schemes were tested to verify the 2-digit accuracy in the numerical results.) The partial differential equations (2) were discretized using first-order upwind finite differences – the term  $(u + f)u_x$  was treated explicitly, while  $vu_y$  and  $u_{yy}$  were treated implicitly in time. The adjoint equations (8) were discretized to be the numerical adjoints of the discretization of (2). A two-level checkpointing scheme[17] is used to generate  $u$  and  $v$  needed to integrate the adjoint variables backwards in  $t$ . This procedure ensures that for any discretized  $f(t)$ , the numerical solution satisfies the discretized versions of (2), (3), (8) and (9), and the first variation  $\delta\mathcal{L}/\delta f$  from (10) can be calculated. The optimization in  $f$  is achieved using gradient descent by starting from an initial guess  $f^0(t) = 1$ , and iteratively updating it as  $f^{n+1}(t) = f^n(t) + s(\delta\mathcal{L}/\delta f)$ , for a fixed small number  $s$ . (The multiplier  $\lambda$  in (10) is chosen so that (4) is satisfied by  $f^{n+1}$ .) We find this procedure to converge, as  $\delta\mathcal{L}/\delta f$  approaches 0, presumably because the optimum is unique.

The results of the computation are shown in Figure 2. The analytical solution[20] derived for  $\epsilon \rightarrow 0$ ,

$$f(t) = f_0(t) = Ct^{1/4}(1-t)^{1/4} \text{ and} \tag{12a}$$

$$\mathcal{W}_{\min} = \mathcal{W}_{0,\min} \approx 1.014, \tag{12b}$$

where  $C \approx 1.62$ , approximates the solution for finite  $\epsilon$  upto a value of about 0.5. As  $\epsilon$  increases beyond, the optimal  $f(t)$  departs from  $f_0(t)$  while  $\mathcal{W}_{\min}$  rises above  $\mathcal{W}_{0,\min}$ . In particular,  $f(t)$  appears to start from  $f(0) = 0$  and end at  $f(1) = 0$  but flattens out in the middle. As  $\epsilon$  rises to values  $\gtrsim 5$ ,  $f(t)$  approaches unity, except for near the start and the end. In other words, the optimum kinematics to cover a distance  $D \gg L$  in time  $T$  is to cruise at the average speed  $U \approx D/T$ , except to start and stop. For  $\epsilon \gg 1$ ,  $\mathcal{W}_{\min}$  is also observed to rise  $\propto \epsilon^{1/2}$ .

The following argument rationalizes these observations. The drag for a flat plate moving at steady speed  $U$  is given by[21]  $0.664\sqrt{\mu\rho U^3 L}$ , and consequently, the work done to move the plate is  $\tilde{\mathcal{W}}_\infty = 0.664T\sqrt{\mu\rho U^5 L}$ . Consider covering the distance  $D$  in two stages of duration  $aT$  and  $(1-a)T$  moving with speeds  $U_1 = bU/a$  and  $U_2 = (1-b)U/(1-a)$ , respectively, for constants  $a$  and  $b$  between 0 and 1. Assuming that steady state is reached

much faster than the duration of each segment, the modified kinematics incurs the work

$$0.664T\sqrt{\mu\rho U^5 L}\left(\frac{b^{5/2}}{a^{3/2}} + \frac{(1-b)^{5/2}}{(1-a)^{3/2}}\right). \quad (13)$$

This work is minimized when  $b = a$ , or  $U_1 = U_2 = U$ . In other words, because of the convexity of  $U^{5/2}$  with respect to  $U$ , the penalty incurred in the work done when traveling fast outweighs the benefits accrued when traveling slower, explaining why the optimum avoids slow modulation of the speed. Converting  $\tilde{\mathcal{W}}_\infty$  to dimensionless terms yields,  $\mathcal{W}_{\min} \approx 0.664\epsilon^{1/2}$  for  $\epsilon \gg 1$ , agreeing up to the leading order with the results of the computations as shown in Figure 2(a).

It is readily seen why the optimal profile avoids an impulsive start and stop. At very early times (and also close to the finish line) owing to the development of the viscous boundary layer, the unsteady inertia  $u_t$  and shear viscosity  $u_{yy}$  in (2) dominate, while advection  $\epsilon(u+f)u_x + \epsilon v u_y$  is negligible. Therefore, in the first variation condition (10), the dominant balance is between  $u_y$  and  $\alpha_y$ . For an impulsive start, the initial shear stress profile on the plate,  $u_y|_{y=0}$ , asymptotically behaves as  $f(0)/\sqrt{\pi t}$  due to the growth of the boundary layer thickness proportional to  $\sqrt{t}$ . The adjoint dynamics, due to their backwards evolution in time, does not “know” about the impulsive start, and therefore cannot generate an  $\alpha_y$  that matches this asymptotic behavior. Therefore, for small  $t$ , one can always reduce the work done by eliminating the impulsive start (and similarly for an impulsive stop).

In fact, as in the analytical solution for vanishing  $\epsilon$  in (12), we find that for finite  $\epsilon$  the optimal starting and stopping dynamics behave proportional to  $t^{1/4}$  and  $(1-t)^{1/4}$ , respectively. This is observed in the numerical solution for over four orders of magnitude in  $t$ , as shown in Figure 3. Near the starting and stopping time, the advection is negligible and the optimal kinematics are governed by the viscous diffusion of momentum within the fluid, which causes this behavior[20].

Finally, we observe that for  $\epsilon \gg 1$ , the starting and stopping dynamics as a function of  $\epsilon t$  are independent of  $\epsilon$ , as seen in Figure 4. (Here  $\epsilon t$  is the ratio of the distance covered when travelling at speed  $D/T$  to the plate length.) For  $\epsilon \geq 5$ , these optimal starting and stopping dynamics approach successively closer to limiting curves. These limiting curves denote the work-minimizing kinematics for the flat plate to attain a constant cruising speed from rest and to stop from the cruising motion, respectively. These starting and stopping kinematics depend only on the cruising speed, which we non-dimensionalize to unity, and

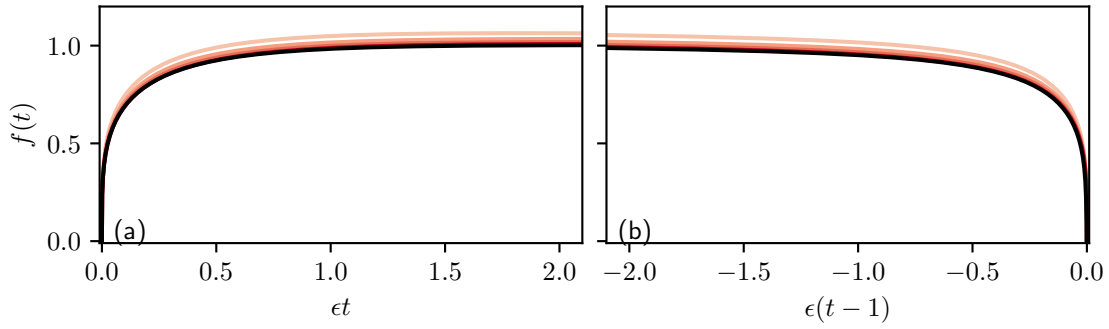


FIG. 4. Optimal starting and stopping kinematics. (a) The start-up dynamics of optimal kinematics for  $\epsilon=5, 10, 20$  and  $50$  (same color code as in Figure 2) plotted against  $\epsilon t$ . Black curve shows the optimal starting kinematics. (b) Same as (a) but for stopping kinematics.

do not depend on the distance travelled  $D$  or the time taken  $T$ . The governing equations to determine the limiting start-up dynamics are identical to the ones developed so far with the following exceptions. The  $t$  and  $y$  variables are rescaled as  $\epsilon t = t'$  and  $y\sqrt{\epsilon} = y'$ , and formally  $t'$  ranges from 0 to  $\tau \rightarrow \infty$  (all the integrals in (7) are now over the semi-infinite time interval). The distance travelled condition (4) is replaced by

$$\mathcal{D}' = \lim_{\tau \rightarrow \infty} \frac{1}{\tau} \int_0^{\tau} f(t) dt - 1 = 0. \quad (14)$$

An additional constraint that the final velocity profile approaches the Blasius steady-state profile  $u_s(x, y, t)$  with  $u_s(x \in P, y = 0, t) = -1$  is added. Imposing a target final state for  $u$  implies that the condition for starting the backwards time-integration of  $\alpha$  must be determined as part of the solution. This condition is trivially determined to be the steady solution of (8) with  $u = u_s$  and  $\alpha(x \in P, y = 0, t) = 1$ . The numerical procedure outlined earlier then yields the optimum start-up kinematics.

For the optimum stopping kinematics, the time variable  $t'$  is shifted so that the final time is zero. The initial state for  $u$  is  $u_s$ , and the final state is unknown. Therefore,  $\alpha = 0$  at  $t' = 0$  holds. The distance travelled condition is replaced by

$$\mathcal{D}'' = \lim_{\tau \rightarrow \infty} \frac{1}{(-\tau)} \int_{-\tau}^0 f(t) dt - 1 = 0. \quad (15)$$

Following the aforementioned numerical procedure then yields the optimal stopping kinematics. Figure 4 shows that the profiles for finite but large  $\epsilon$  converge to the optimal starting and stopping kinematics.

The work-minimizing kinematics for large  $\epsilon$  can now be better expressed using integrals of the optimal starting and stopping kinematics. Because  $f \leq 1$  for the optimal starting kinematics, the distance travelled by the plate always lags behind one moving with cruising speed. For the starting kinematics,  $\int_0^\infty (f(t') - 1) dt' = -0.12$ , implying that by the time steady cruising at speed  $U_c$  is reached, the optimal kinematics lags a distance  $0.12L$  behind. Using similar integrals, we find that the optimal starting kinematics consumes work  $0.40 \times \sqrt{\rho\mu U_c^3 L^3}$  in addition to the work accumulated linearly with elapsed time  $\tilde{t}$  at the cruising speed,  $0.664\tilde{t}\sqrt{\mu\rho U_c^5 L}$ . Similarly, an additional distance of  $0.2L$  is lost during the optimal stopping kinematics, and  $0.39 \times \sqrt{\rho\mu U_c^3 L^3}$  of work is recovered from the kinetic energy of the surrounding flow. Thus, the profile constructed by patching together the optimal starting and stopping kinematics with cruising speed  $U_c$  traverses a distance equal to  $U_c T - 0.32L$  and consumes total work of  $0.01\sqrt{\rho\mu U_c^3 L^3} + 0.664T\sqrt{\mu\rho U_c^5 L}$ . Equating the distance travelled to  $D$  yields a correction to the cruising speed  $U_c = (D + 0.32L)/T$ , which in dimensionless terms is  $f = 1 + 0.32/\epsilon$ . Similarly, substituting the cruising speed in expression for the work-done yields the two-term approximation  $\mathcal{W}_{\min} \sim 0.664\epsilon^{1/2} (1 + 0.81\epsilon^{-1})$ .

These results, in essence, apply to motion of streamlined bodies such as airfoils where the drag arises from skin friction. A limitation of this calculation is that motion of the plate perpendicular to its surface, or motion of bluff bodies that will generate form drag, is not considered. Despite the limitations, we list two elements of this work that are useful for the broader kinematic optimization community. First, the problem treated here poses a test case for computational kinematic optimization implementations. The  $\tilde{t}^{1/4}$  starting and  $(T - \tilde{t})^{1/4}$  stopping kinematics are specific singular behaviors that accurate implementations should reproduce. These functional forms also constitute useful library elements for model identification algorithms based on sparse regression[22]. Second, the proof for the uniqueness of work-minimizing kinematics transcends beyond the specific example presented here and applies more generally to all cases where (i) the fluid starts from rest and (ii) the dissipation is quadratic. The central element of the proof is the positive definiteness of kinetic energy and dissipation, which applies even in the presence boundary layer separation and form drag. Powerful proofs of uniqueness may be constructed for optimization over complicated kinematic space even when the flow is governed by the Navier-Stokes equations. Based on this, it appears that a gradient descent for determining, say, the optimal C-start kinematics of fish larvae would yield the result with much less computation than evolutionary algorithms[13].

These exercises we leave for the future.

---

- [1] G. J. Berman and Z. J. Wang, *Journal of Fluid Mechanics* **582**, 153 (2007).
- [2] D. Tam and A. E. Hosoi, *Proceedings of the National Academy of Sciences* **108**, 1001 (2011).
- [3] S. Alben, L. A. Miller, and J. Peng, *Journal of Fluid Mechanics* **733**, 100 (2013).
- [4] S. Kern and P. Koumoutsakos, *Journal of Experimental Biology* **209**, 4841 (2006).
- [5] D. Tam and A. E. Hosoi, *Physical Review Letters* **98** (2007).
- [6] S. Michelin and E. Lauga, *Physics of Fluids* **22**, 111901 (2010).
- [7] S. Michelin and E. Lauga, *Physics of Fluids* **23**, 101901 (2011).
- [8] C. Eloy and E. Lauga, *Physical Review Letters* **109** (2012).
- [9] S. Michelin and E. Lauga, *Journal of Fluid Mechanics* **715**, 1 (2013).
- [10] L. Was and E. Lauga, *Bioinspiration & biomimetics* **9**, 016001 (2014).
- [11] T. D. Montenegro-Johnson and E. Lauga, *Physical Review E* **89** (2014).
- [12] U. Pesavento and Z. J. Wang, *Physical Review Letters* **103** (2009).
- [13] M. Gazzola, W. M. Van Rees, and P. Koumoutsakos, *Journal of Fluid Mechanics* **698**, 5 (2012).
- [14] W. M. van Rees, M. Gazzola, and P. Koumoutsakos, *Journal of Fluid Mechanics* **775**, 178 (2015).
- [15] A. P. Maertens, A. Gao, and M. S. Triantafyllou, *Journal of Fluid Mechanics* **813**, 301 (2017).
- [16] A. Griewank, *Optimization Methods and software* **1**, 35 (1992).
- [17] A. Griewank and A. Walther, *ACM Transactions on Mathematical Software* **26**, 19 (2000).
- [18] Q. Wang, P. Moin, and G. Iaccarino, *SIAM Journal on Scientific Computing* **31**, 2549 (2009).
- [19] G. J. Chandler, M. P. Juniper, J. W. Nichols, and P. J. Schmid, *Journal of Computational Physics* **231**, 1900 (2012).
- [20] S. Mandre, *J. Fluid Mech.* **893**, R4 (2020).
- [21] G. K. Batchelor, *An introduction to fluid dynamics* (1967).
- [22] S. L. Brunton, J. L. Proctor, and J. N. Kutz, *Proceedings of the National Academy of Sciences* **113**, 3932 (2016).